pH Effect on the Photochemistry of 4-Methylcoumarin Phosphate Esters: Caged-Phosphate Case Study

ARTICLE *in* THE JOURNAL OF PHYSICAL CHEMISTRY A · NOVEMBER 2010

Impact Factor: 2.69 · DOI: 10.1021/jp103045u · Source: PubMed

4 AUTHORS, INCLUDING:

A. Jorge Parola
New University of Lisbon
118 PUBLICATIONS **1,810** CITATIONS
SEE PROFILE

Pedro V Baptista
New University of Lisbon
142 PUBLICATIONS **1,867** CITATIONS
SEE PROFILE

João Carlos Lima
New University of Lisbon
143 PUBLICATIONS **2,192** CITATIONS
SEE PROFILE

pH Effect on the Photochemistry of 4-Methylcoumarin Phosphate Esters: Caged-Phosphate Case Study

André Vidal Pinheiro,[†,‡] A. Jorge Parola,[†] Pedro V. Baptista,[‡] and J. C. Lima*[,†]

REQUIMTE, Departamento de Química, Faculdade de Ciências e Tecnologia, Universidade Nova de Lisboa, 2829-516 Caparica, Portugal and CIGMH, Departamento de Ciências da Vida, Faculdade de Ciências e Tecnologia, Universidade Nova de Lisboa, Campus de Caparica, 2829-516 Caparica, Portugal

Received: April 5, 2010; Revised Manuscript Received: October 23, 2010

There are numerous reports of coumarin ester derivatives, in particular phosphate esters, as photocleavable cages in biological systems. Despite the comprehensive analysis of the photocleavage mechanism, studies of 4-methylcoumarin caged phosphates and/or nucleotides were always performed at constant pH. In this work, we present the study of the pH effect on the photochemistry of (7-diethylaminocoumarin-4-yl)methyl phosphate (DEACM−P). Fluorescence and photocleavage quantum yields, as well as the fluorescence decay times were measured as a function of the pH. It was found that the pH produces significant changes in the overall photochemical quantum yield of DEACM−P, and the observed changes are complementary to those obtained from the fluorescence quantum yield. Deprotonation of DEACM−HPO_4^- to yield DEACM−PO_4^{2-}, produces a decrease in the photochemical quantum yield (from 0.0045 to 0.0003) and an increase in the fluorescence quantum yield (from 0.072 to 0.092). Moreover, from the analysis of the decay times, we have also found that hydroxyl ion is not only relevant, but it is mechanistically involved in the photoreaction of DEACM−HPO_4^-.

Introduction

Controlled temporal and spatial release of biomolecules from photolabile precursors, commonly known as caged molecules, has become increasingly valuable for cell and molecular biology studies. The rationale of using caged compounds is straightforward: the molecule of interest is rendered biologically inactive (caged) by chemical modification with a protecting group that can be removed with light by irradiation with a suitable wavelength.[1,2] This promotes the release of the biologically active molecule, generating a time-controlled burst in concentration with tight spatial control.[3] Among the several caging groups reported in the literature,[4,5] coumarin derivatives present a great potential for biological application due to their absorption bands with high extinction coefficients in the visible region of the spectrum, which minimizes the risk of damaging nucleic acids or proteins upon irradiation. In addition, a careful choice of the coumarinic core substitution pattern allows one to fine-tune the absorption and emission maxima in the visible region.[6] There are numerous reports of coumarin derivatives used in biological systems, such as caged peptides,[7] caged phosphates for acidification of membranes,[8] caged glutamate,[9] gene activation using caged RNA,[10] and caged cyclic nucleotides release for activation of cyclic nucleotide-gated (CNG) channels.[11,12]

The first interpretation of the photocleavage mechanism of 4-methylcoumarin esters was suggested by Furuta,[9] where he considered to occur from the triplet state, through a homolytic bond cleavage. Bendig and co-workers[6] excluded the hypothesis of triplet origin due to the absence of phosphorescence at 77 K. The homolytic cleavage was also excluded since no products were detected resulting from hydrogen abstraction by radicals.

It is now generally accepted that the photocleavage of coumarin phosphate esters involves photoheterolysis of the C−O ester bond and subsequent ion-pair separation in a polar solvent, followed by trapping of the coumarinylmethyl carbocation by water.[6] Further studies have shown that the coumarin alcohol photoproduct is, in some cases, formed in the subnanosecond time-range, which is the fastest photodeprotection rate reported so far.[13]

In 2007, in a broader study regarding the characterization of coumarin cages (Cm) with different leaving groups (A), it was proposed that, upon coumarin excitation to S1 excited state, a significant weakening of the Cm-A ester leads to the formation of^1[Cm^+ A^-] ion pair.[14] Stabilization of the carbocation Cm^+ is favored by strong electrodonating substituents in the coumarin moiety, while stabilization of the leaving anions A^- is better accomplished if they present low basicity. Transient ion pair stabilization results in the increase of the observed rate of product formation and also in photochemistry efficiency, since recombination of the ion pair is disfavored. Despite the comprehensive analysis of the photocleavage mechanism, the photochemical studies of 4-methylcoumarin caged phosphates and nucleotides were always performed at constant pH, independently on the number of prototropic species in equilibrium. Among the species present in solution, it is important to clarify which ones are responsible for the photochemistry and evaluate the impact of pH in the photorelease quantum yield, mainly since the microenvironments inside cells might be difficult to predict in the case of in vivo applications.

Experimental Methods

General Information. All chemicals were purchased from Sigma Aldrich in the highest purity available and used without

* To whom correspondence should be addressed. Tel: +351 212 948 575. Fax: +351 212 948 550. E-mail: lima@dq.fct.unl.pt.

[†] REQUIMTE, Departamento de Química, Faculdade de Ciências e Tecnologia, Universidade Nova de Lisboa.

[‡] CIGMH, Departamento de Ciências da Vida, Faculdade de Ciências e Tecnologia, Universidade Nova de Lisboa.

10.1021/jp103045u
Published on Web 11/19/2010

further purification. THF was refluxed with sodium/benzophenone and distilled before use. A Hitachi-Merck HPLC L6200A Pump with an L-4500 Diode Array Detector using a RP-18 end-capped (Purospher Star, Merck) analytical column (4.6 mm ×15 mm, 5 μm) was employed for DEACM−P and DEACM−OH detection in photochemical quantum yield determinations. Eluent A was trietylammonium acetate buffer in water, 5 mM, pH 6.9; eluent B was methanol. The gradient used started with 40% of B in A; with an increase to 100% B after 8 min, and finished after 15 min at 100% of B. Separations were run at a flow rate of 0.9 mL/min, and the column temperature was 35 °C. The ^{1}H NMR spectra at 298.0 K were obtained on a Bruker AMX400 operating at 400.13 MHz. The ESI mass spectra were run on a Platform II spectrometer from Micromass. All solutions were protected from light and DEACM−P manipulations were performed in a dark chamber under red-light illumination. All spectroscopic measurements and irradiations were performed in 3 mL quartz fluorescence cuvettes (1 cm optical path) at 21 °C. Absorption spectra were recorded on a Varian Cary Bio 100 UV−visible spectrophotometer. Fluorescence measurements of aerated solutions were performed on a Horiba-Jobin-Yvon SPEX Fluorolog 3.22 spectrofluorimeter. All emission spectra were collected with 1.5 nm slit bandwidth for excitation and emission, with correction files.

DEACM Derivatives: Synthesis and Purification. 7-Diethylamino-4-hydroxymethylcoumarin (DEACM−OH) and (7-diethylaminocoumarin-4-yl)methyl phosphate (DEACM−P) were synthesized as described by Schonleber et al.[15]

For DEACM−OH, ^{1}H NMR (400 MHz, $CDCl_3$) δ 7.32 (d, J = 9.2 Hz, H5), δ 6.56 (d, J = 9.2 Hz, H6), δ 6.50 (s, H8), δ 4.83 (d, J = 5.6 Hz, $\underline{CH_2}$−OH), δ 3.40 (q, J = 7.2 Hz, N−$\underline{CH_2}$−CH_3), δ 1.19 (t, J = 6.8 Hz, N−CH_2−$\underline{CH_3}$); MS (ESI+) m/z $[M+H]^+$ = 248.3; calculated for $C_{14}H_{18}NO_3$ 248.30.

For DEACM-P, ^{1}H NMR (400 MHz, D_2O) δ 7.86 (d, J = 8.4 Hz, H5), δ 7.60 (s, H8), δ 7.45 (d, J = 8.0 Hz, H6), δ 6.72 (s, H3), δ 5.13 (d, J = 7.2 Hz, $\underline{CH_2}$−O−P), δ 3.62 (q, J = 7.2 Hz, N−$\underline{CH_2}$−CH_3), δ 1.04 (t, J = 6.8 Hz, N−CH_2−$\underline{CH_3}$).

Absorption and Emission Titrations. Absorption and emission titrations were carried out in 10 mM phosphate buffer, initial pH 6.9. Solutions with approximate 0.1 absorbance units at this pH were prepared. The pH was then adjusted with HCl and the titration was performed via addition of NaOH. Absorption spectra were corrected for baseline and dilution. Corrected absorbance values at 385 nm were plotted as function of pH. Fitting of absorption titration curve for the acid−base equilibrium between two species to experimental data was processed, using the following equation:

$$A_T = \varepsilon(A) \times [A]_0 \times \frac{K_a}{K_a + [H^+]} \times l + \varepsilon(HA^+) \times [A]_0 \times \frac{[H^+]}{K_a + [H^+]} \times l \quad (1)$$

A_T is the total absorbance at 385 nm; ε(A) and $\varepsilon(HA^+)$ are the extinction coefficients of the unprotonated and protonated species, respectively; K_a is the equilibrium constant; l is the optical path length (1 cm); and $[A]_0$ is the initial concentration. K_a and $\varepsilon(HA^+)$ values were used as adjustable parameters for the fitting. Emission spectra were collected with excitation at 325 nm (isosbestic point) and corrected for light absorption at this wavelength. The total emission band area was normalized at pH 8.2 for fluorescence quantum yield. For DEACM−OH, fitting of an emission titration curve of the equilibrium between two species to experimental data was processed, using the following equation:

$$I_T = \Phi_f(A) \times \frac{K_a}{K_a + [H^+]} \times I_0 + \Phi_f(HA^+) \times \frac{[H^+]}{K_a + [H^+]} \times I_0 \quad (2)$$

I_T is the integrated emission area with excitation at 325 nm at each pH value; I_0 is the integrated emission area with excitation at 325 nm at the highest pH value measured; Φ_f(A) and $\Phi_f(HA^+)$ are the fluorescence quantum yields of the protonated and deprotonated species, respectively; and K_a is the equilibrium constant. K_a and $\Phi_f(HA^+)$ values were used as adjustable parameters for the fitting. For DEACM−P, it is necessary to consider three prototropic species to fit the emission titration curve:

$$I_T = \frac{\Phi_f(A^{2-}) \times I_0}{1 + \frac{K_{a1}}{[H^+]} + \frac{K_{a1} \times K_{a2}}{[H^+]^2}} + \frac{\Phi_f(HA^-) \times I_0}{1 + \frac{[H^+]}{K_{a1}} + \frac{K_{a2}}{[H^+]}} + \frac{\Phi_f(H_2A) \times I_0}{1 + \frac{[H^+]}{K_{a2}} + \frac{[H^+]^2}{K_{a1} \times K_{a2}}} \quad (3)$$

$\Phi_f(A^{2-})$, $\Phi_f(HA^-)$, and $\Phi_f(H_2A)$ are fluorescence quantum yields of the three species and K_{a1} and K_{a2} are the respective equilibrium constants. K_{a1}, K_{a2}, $\Phi_f(HA^-)$, and $\Phi_f(H_2A)$ values were used as adjustable parameters for the fitting.

Fluorescence and Photochemical Quantum Yield Determinations. Fluorescence quantum yields (Φ_f) were determined by the relative method using Coumarin 1 (7-diethylamino-4-methylcoumarin) degassed solution in ethanol (Φ_f = 0.730) as standard.[16] The optical densities of DEACM−P and DEACM−OH solutions in 10 mM Tris-acetate buffer at pH 8.2 and that of the standard were adjusted to identical values in the range of 0.08 to 0.12, at excitation wavelength of 386 nm. Correction for the refractive index was included in the calculation.

DEACM−P photochemical quantum yields (Φ_{chem}), defined as the number of DEACM−OH molecules formed by each photon absorbed by DEACM−P, were carried out in 10 mM Tris-acetate buffer at each indicated pH. Sequential irradiation times of DEACM−P solution were carried out and the resulting DEACM−P and DEACM−OH quantities determined by HPLC (peak area quantification, corrected for molar absorptivities). Irradiations were carried out in a Horiba−Jobin−Yvon Spex Fluorolog 1681 Spectrometer with a 150 W xenon arc lamp, monochromated for the excitation wavelength (385 nm, 18 nm slit bandwidth). The actinometry of the irradiation setup was performed using the micro version of potassium ferrioxalate actinometer[17] and an intensity of $I_0 = 1.79 \times 10^{-7}$ einstein·min^{-1} was measured. Photochemical quantum yields were calculated as the slope of the linear regression obtained by plotting DEACM−OH moles formed ($\Delta n_{DEACM-OH}$) as a function of irradiation time (Δt), according to the following equation:

$$\Delta n_{DEACM-OH} = \Phi_{chem} \times I_0 \times (1 - 10^{A_T}) \times \Delta t \quad (4)$$

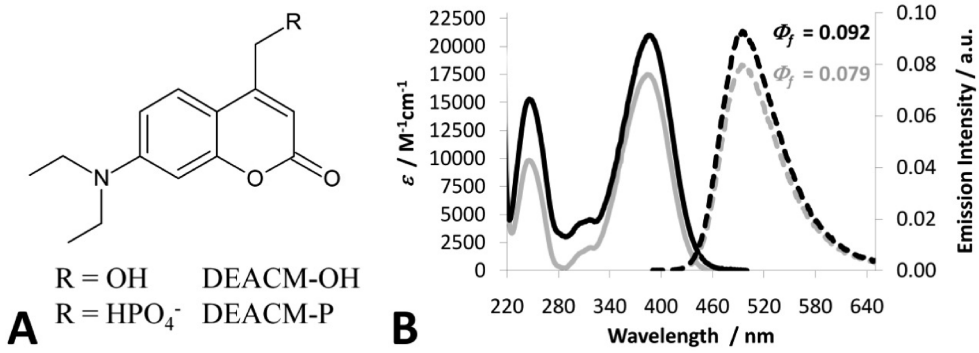

Figure 1. (A) DEACM−OH and DEACM−P structure. (B) Absorption (full line) and emission spectra (dashed line) of DEACM−OH (in gray) and DEACM−P (in black) in Tris-acetate buffer, 10 mM, pH 8.2. Absorption spectra are represented in molar absorptivities and emission spectra normalized for each compound fluorescence quantum yield. Emission spectra were obtained by excitation at 385 nm.

The fraction of light absorbed by the solution ($1-10^{-A_T}$) was calculated from the absorption spectra, where A_T is the total absorbance of the solution at the irradiation wavelength. The same calculation was processed for the disappearance of DEACM−P. Photochemical quantum yields used in the calculation of the photochemical rate constants are the mean value of the ones obtained for DEACM−OH formation and DEACM−P disappearance.

Time-Resolved Fluorescence Spectroscopy Measurements. Fluorescence decays were measured using a home-built picosecond time-correlated single photon counting (TCSPC) apparatus described elsewhere.[18] The excitation source consists of a picosecond Spectra Physics mode-lock Tsunami Laser (Ti:Sapphire) Model 3950 (repetition rate of about 82 MHz, tuning range 700−1000 nm), pumped by a Millennia Pro-10s, frequency-doubled continuous wave (CW), diode-pumped, solid-state laser (λ_{em} = 532 nm). A harmonic generator model GWU-23PS (Spectra Physics) is used to produce the second and third harmonic from the Ti:Sapphire laser exciting beam frequency output. The samples were measured with excitation at 425 nm and the horizontally polarized output beam from the GWU (second harmonic) was first passed through a ThorLabs depolarizer (WDPOL-A) and after by a Glan-Thompson polarizer (Newport 10GT04) with vertical polarization. Emission at 90° geometry collected at magic angle polarization was detected through an Oriel Cornerstone 260 monochromator by a Hamamatsu microchannel plate photomultiplier (R3809U-50). Signal acquisition and data processing were performed employing a Becker & Hickl SPC-630 TCSPC module. Fluorescence decays and the instrumental response function (IRF) where collected using 4096 channels in a 0.814 ps per channel scale, until 5×10^3 counts at maximum were reached. The full width at half-maximum of the IRF was about 22 ps and was highly reproducible with identical system parameters. Fluorescence decays were collected at 520 nm. The obtained fluorescence decays were deconvoluted using the modulating functions method.[19,20]

Flash Photolysis Spectroscopy Measurements. Flash photolysis experiments were performed in a LKS.60 ns laser photolysis spectrometer from Applied Photophysics, with a Brilliant Q-Switch Nd:YAG laser from Quantel, using the third harmonic (λ_{exc} = 355 nm, laser pulse intensity $\sim 3.34 \times 10^{-8}$ Einstein cm^{-2} with fwhm 6 ns). A 150 W xenon arc lamp was used as monitoring lamp to analyze transient absorption. A flow flash setup (Applied Photophysics SX.18MV-R) was used to change the sample solution after each shot, due to the photolabile nature of DEACM−P. The coumarin solutions studied presented absorption of 0.3 at 355 nm, in 10 mM Tris-acetate buffer. Decays were obtained using a 2.0 nm slits, and photomultiplier sensitivity adjusted to a light-level of 260 ± 10 mV. Transient spectra of aerated solutions were measured at each 10 nm, from 300 to 600 nm. For the pH dependent studies, independent decay measurements at 500 nm were performed in quintuplicate. Decay analysis was performed by adjusting a single-exponential decay fitting curve to experimental decay using OriginPro 8 software.

Results and Discussion

Ground State Properties of DEACM−OH and DEACM−P. Recently, we demonstrated the use of 7-diethylamino-4-methylcoumarin caged-nucleotides for the control of in vitro transcription reactions.[21] We observed that the irradiation times necessary for total cleavage of DEACM caged-nucleotides were unexpectedly altered depending on the buffer used. For that reason, we decided to study the influence of pH on the photocleavage mechanism of (7-diethylaminocoumarin-4-yl)methyl phosphate (DEACM−P) (Figure 1A). To isolate the pH effect in the photochemistry of DEACM−P, a systematic comparison with 7-diethylamino-4-hydroxymethylcoumarin (DEACM−OH) (Figure 1A) was performed.

Figure 1B shows the absorption and emission spectra of DEACM−OH and DEACM−P, obtained in 10 mM Tris-acetate buffer at pH 8.2. Both, DEACM−OH and DEACM−P, present two absorption bands with maxima at 246 and 385 nm, and 246 and 388 nm, respectively. The low energy transitions observed in the absorption spectra, at 385 and 388 nm, are $\pi\pi^*$ transitions with strong CT character, involving the transfer of charge between the amino group in the 7- position and the coumarinic core.[22] The phosphate derivative presents a slightly higher extinction coefficient. Both compounds present a single emission band with maxima around 500 nm and similar fluorescence quantum yields (0.079 for DEACM−OH and 0.092 for DEACM−P).

The pH dependence of the DEACM−OH absorption spectra is shown in Figure 2A. At very acidic pH, protonation of the amine leads to the disappearance of the charge transfer band at 385 nm, resulting in two absorption bands with maxima around 265 and 310 nm. At increasing pH, conversion of protonated to deprotonated form leads to the presence of two isosbestic points at 266 and 325 nm. From the spectrophotometric titration, a pK_a value of 3.2 can be determined that corresponds to the acid−base equilibrium between DEACM−OH and HDEACM−OH^+ protonated at the 7-diethylamino group.

For DEACM−P, a similar variation in the absorption spectra as function of the pH is obtained with identical pK_a value (Figure

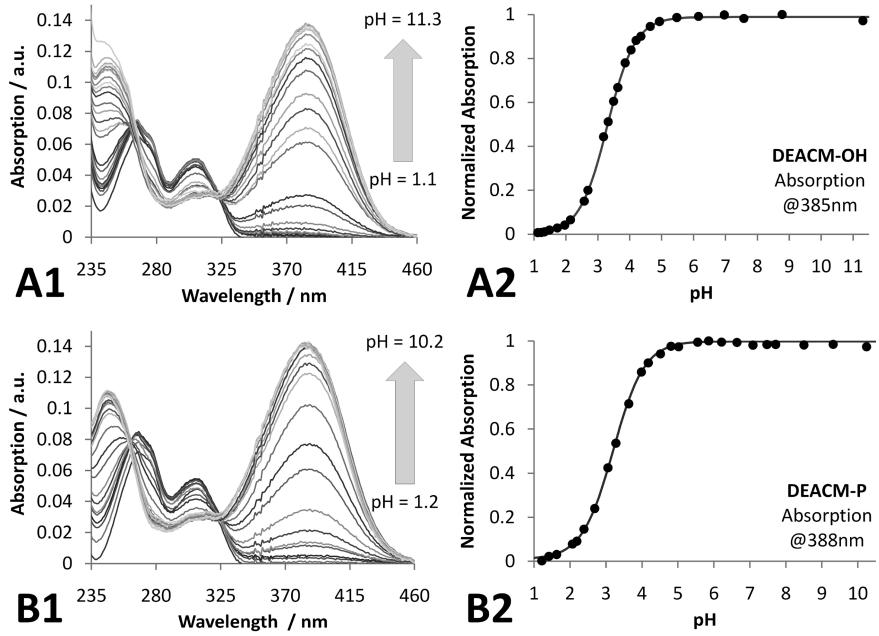

Figure 2. (A) DEACM−OH spectrophotometric titration in 10 mM Tris-phosphate buffer. 1: Absorption spectra at each pH value ranging from 1.1 to 11.3 with increasing addition of NaOH. Total DEACM−OH concentration used was 8.0 μM. 2: Normalized absorbance at 385 nm (dots) and fitting for the equilibrium between two species (line; see eq 1). (B) DEACM−P spectrophotometric titration in 10 mM Tris-phosphate buffer. 1: Absorption spectra at each pH value ranging from 1.2 to 10.2 with increasing addition of NaOH. Total DEACM−P concentration used was 6.7 μM. 2: Normalized absorbance at 388 nm (dots) and fitting for the equilibrium between two species (line; see eq 1).

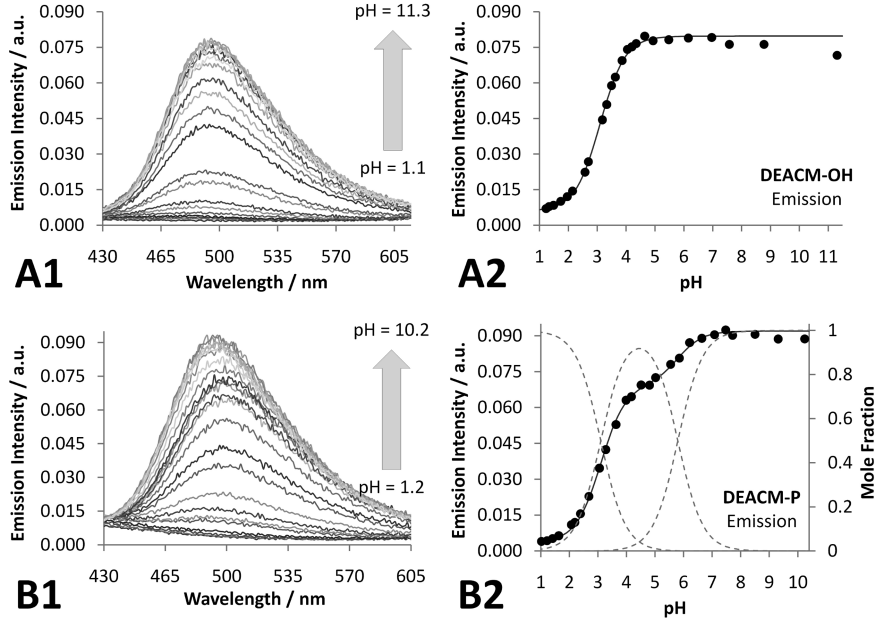

Figure 3. (A) DEACM−OH fluorimetric titration in 10 mM Tris-phosphate buffer. 1: Emission spectra obtained with excitation at 325 nm at each pH value ranging from 1.1 to 11.3. Fluorescence intensities are normalized for fluorescence quantum yield measured at pH 8.2. 2: Fluorescence intensities obtained by integrated emission area normalized for fluorescence quantum yields (dots) and fitting for the equilibrium between two species (line; see eq 2). (B) DEACM-P fluorimetric titration in 10 mM Tris-phosphate buffer. 1: Emission spectra obtained with excitation at 325 nm at each pH value ranging from 1.2 to 10.2. Fluorescence intensities are normalized for fluorescence quantum yield measured at pH 8.2. 2: Fluorescence intensities obtained by integrated emission area normalized for fluorescence quantum yields (dots) and fitting for the equilibrium between three species (dark gray line; see eq 3). Dashed light gray lines represent mole fractions of the three species in equilibrium.

2B). Therefore, the presence of a phosphate group does not affect the acid−base equilibrium involving the amine in position 7. Additionally, the first deprotonation of the phosphate group is expected to occur at more acidic pH (pK_a = 1.54 for the monomethyl phosphate ester[23]) and cannot account for the observed spectral changes. Moreover, at neutral pH, where deprotonation of the second phosphate group is expected, no spectral changes were observed. The protonation degree of the phosphate group does not seem to affect the absorption spectrum.

Emission Dependence on pH. Fluorescence titration of DEACM−OH fully corroborates the results obtained by absorption spectroscopy, i.e., as the amine-protonated species is produced at more acidic pH values, a decrease in the fluorescence intensity is observed (Figure 3A). This corroborates that the emission arises from the charge transfer state that is absent in the amine protonated form (Figure 4A). A pK_a value of 3.2 is obtained and no evidence for other excited state pH dependent processes was found.

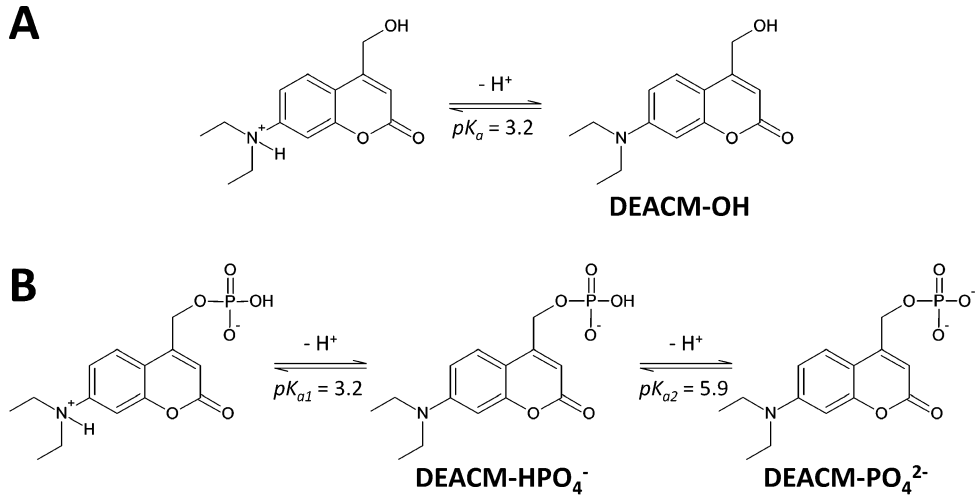

Figure 4. DEACM−OH (A) and DEACM−P (B) acid−base equilibria. It was considered that the first deprotonation of DEACM−P phosphate group occurs at a lower pH value than 1.5.[23]

A different behavior was observed for DEACM−P: at very acidic pH, emission decreases similar to what is observed for DEACM−OH due to the protonation of the amine; however, at higher pH values, an additional dependence of the emission intensity on the pH was found, indicating the presence of a second equilibrium that is not observed in the titration followed by absorption spectroscopy (Figure 3B). The first equilibrium is clearly associated with the protonation of the 7-diethylamino group with a pK_{a1} of 3.2, as determined by the absorption titration. The second equilibrium occurs at pH 5.9, leading to a significant increase in the fluorescence quantum yield. This increase is most probably related to the second deprotonation of the phosphate group, which, in the case of the methyl phosphate ester, is expected to occur at pK_{a2} = 6.31.[23] Considering the conversion between three species (Figure 4B), it is possible to calculate the mole fraction distribution as function of pH for DEACM−P (Figure 3B2).

Dependence of DEACM−P Photochemistry on pH. It is well-known that irradiation at the lower energy transition leads to the photocleavage of coumarin phosphate esters through heterolysis of the C−O ester bond followed by hydroxylation of the coumarinylmethyl carbocation, which in the case of DEACM−P leads to phosphate ion and DEACM−OH as photoproducts.[6,13,14]

The photochemistry quantum yields of phosphate cleavage upon irradiation at 385 nm were calculated independently through determination of DEACM−P disappearance and DEACM−OH appearance. Separation and quantification of DEACM−OH and DEACM−P for each irradiated sample was performed by HPLC. No other photoproduct was detected, confirming DEACM−OH to be the only significant product obtained, as previously reported.[6] Furthermore, quantum yields calculated through DEACM−P disappearance or DEACM−OH formation were found to be identical within the experimental error. Degassing of the solutions did not produce noticeable effects on the photochemical quantum yields, as it would be expected from the short-lived singlet state from where photochemistry derives.[13,14] Additionally, increasing DEACM−P concentrations does not affect the photochemical quantum yield (data not shown).

The pH, however, produces significant variations in the photochemical quantum yields (Figure 5). The observed changes are complementary to those obtained from the fluorescence quantum yield, i.e., Φ_{chem} decreases with the disappearance of

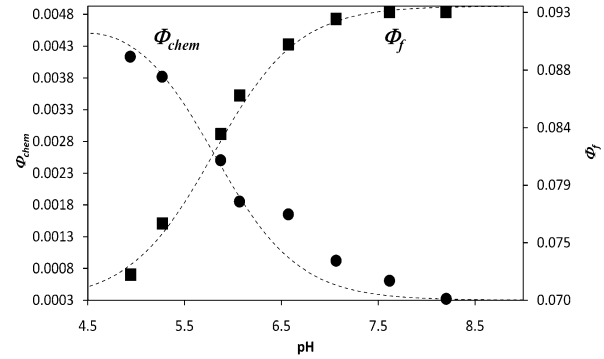

Figure 5. Photochemical (●) and fluorescence (■) quantum yields of DEACM−P as function of pH values in 10 mM Tris-acetate buffer. Dashed gray lines represent mole fraction distribution of DEACM−HPO_4^- and DEACM−PO_4^{2-} equilibrium, obtained from the fluorimetric titration (pK_{a2} = 5.9).

the DEACM−HPO_4^- species to yield DEACM−PO_4^{2-}. The DEACM−HPO_4^- species, predominant between pH = 3 and pH = 6, is characterized by a higher Φ_{chem} (0.0041 at pH 5.2 vs 0.0003 at pH 8.6) and lower Φ_f (0.072 at pH 5.2 vs 0.092 at pH 8.6). These results show that, although the phosphate protonation does not affect the light absorption, it significantly alters the excited state deactivation pathways.

Time resolved fluorescence spectroscopy of DEACM−OH in 10 mM Tris-acetate buffer yielded fluorescence decays well fitted to a single-exponential law with a decay-time of 517 ps, which does not vary with the pH between 5.3 and 8.4 (Figure 6A, gray squares). For DEACM−P in 10 mM Tris-acetate, biexponential decays were obtained (see Supporting Information, SI 1). The longer decay-time, with an average value of 657 ps, shows little dependence on proton concentration, whereas the short decay-time shows a 2-fold decrease with increasing pH (Figure 6A) (from 502 to 256 ps, between pH 5.3 and 8.4, respectively).

The pre-exponential factors (amplitudes) associated to the decay-times reproduce the mole fraction distribution of DEACM−HPO_4^- and DEACM−PO_4^{2-}, determined by fluorimetric titration, and allow a straightforward assignment of the decay components.

Re-excitation of the photoproduct was a concern during the measurement of the decays, since the obtained curves could be a mixture of starting material and photoproduct decays. Therefore, we have performed consecutive decay measurements of

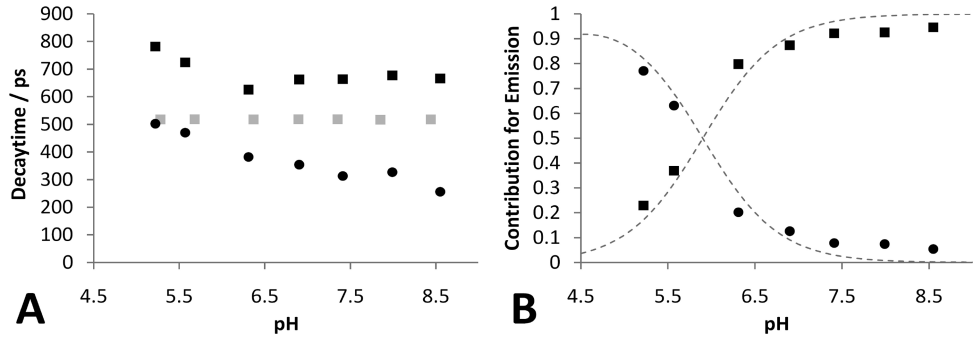

Figure 6. Time resolved fluorescence measurements of DEACM−OH and DEACM−P compounds as function on pH, in 10 mM Tris-acetate buffer, with excitation at 425 nm and collection at 520 nm. (A) Decay-times of DEACM−OH (■) obtained through monoexponential analysis and DEACM−P (■ and ●) obtained through biexponential analysis. (B) Normalized contribution for emission of DEACM−P decay given by the product of the decay-time and pre-exponential factor for each component (■ for the longer component and ● for the shorter component). Dashed gray lines represent mole fraction distribution of DEACM−HPO_4^- and DEACM−PO_4^{2-} obtained from the fluorimetric titration ($pK_{a2} = 5.9$).

TABLE 1: Photophysical and Photochemical Properties of DEACM−OH and DEACM−P in 10 mM Tris-Acetate Buffer at 21°C

	λ_{max} (Abs/nm)	λ_{max} (Em /nm)	Φ_f	Φ_{chem}	τ (ps)	k_f (s^{-1})	k_{chem} (s^{-1})	k_{nr} (s^{-1})
DEACM−OH	385	493	0.079		517	1.5×10^8		1.8×10^9
DEACM−PO_4^{2-}	389	497	0.092	2.9×10^{-4}	667	1.4×10^8	4.4×10^5	1.4×10^9
DEACM−HPO_4^-			0.071[a]	4.1×10^{-3} [a]	[b]		[c]	

[a] Φ_f and Φ_{chem} for DEACM−HPO_4^- at pH 5.2; at higher pH values both quantum yield for this species could not be accurately determined. [b] See Figure 6. [c] Different kinetic model was applied to DEACM−HPO_4^-; see Figure 7 and Scheme 1.

the same solution and analyzed them, focusing on possible variations in the decay profile with irradiation time. Four consecutive decay measurements (5 *k*counts each) were performed at pH = 5.22 and at pH = 8.55. At pH = 8.55, the decay times and amplitudes show deviations below 3% while at pH = 5.22, the amplitude associated with the longer decay time increases 20% after four consecutive measurements. These data are compatible with the formation of photoproduct at pH = 5.22 upon laser irradiation (but not at pH = 8.55), which is being excited in consecutive pulses and contributing to the decay. The first 5 *k* counts were assumed to include only residual (<5%) contribution of the photoproduct. The good correlation between the pH dependence of the amplitudes and the pH dependence of the molar fractions obtained for DEACM−HPO_4^- and DEACM−PO_4^{2-} (from the fitting of the fluorescence titration data), corroborates this assumption.

The longer decay-time, dominant at higher pH values, is assigned to the fully deprotonated species DEACM−PO_4^{2-} while the shorter and pH dependent decay-time is assigned to DEACM−HPO_4^- (Figure 6B). Although DEACM−PO_4^{2-} could deactivate through cleavage of the O−P ester bond leading to DEACM−OH formation even with very low quantum yield ($\Phi_{chem} = 0.0003$), the decay-time associated to DEACM−PO_4^{2-} is slightly longer than that obtained for DEACM−OH (667 ps vs 517 ps), with the fluorescence quantum yields showing the same trend (0.092 vs 0.079, for DEACM−PO_4^{2-} and DEACM−OH, respectively). In other words, at pH = 8 the photochemistry is residual and the decays are dominated by the nonradiative rate constants, 1.4 ns^{-1} for DEACM−PO_4^{2-} and 1.8 ns^{-1} for the photoproduct (Table 1). The alcohol's nonradiative pathway is slightly more efficient, while both compounds are efficiently deactivated by a nonradiative TICT mechanism. The difference in nonradiative rate constants may be related to the presence of an O−H bond in DEACM−OH: the well-known efficiency of the O−H vibration in dumping the excited state energy providing an additional nonradiative pathway for the alcohol photoproduct.

The decay-time of DEACM−PO_4^{2-} does not show noticeable pH dependence, except at pH values where the weight of the

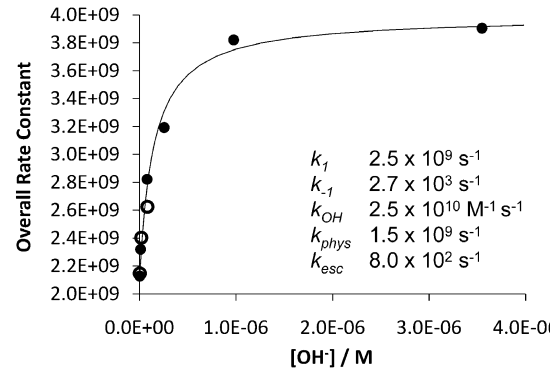

Figure 7. Overall deactivating rate constant of DEACM−HPO_4^- species as function of hydroxyl anion concentration in 10 mM Tris-acetate buffer (●) and 10 mM phosphate buffer (○). The rate constants are given by the reciprocal of the decay time for DEACM−HPO_4^- species at each hydroxyl concentration. Black line represents the nonlinear fitting of the overall deactivating rate constant given by eq 5, based on the kinetic model in Scheme 1. The individual rate constant values presented in the figure were determined after parameter optimization.

SCHEME 1: Kinetic Model for the Photochemistry of DEACM−P Involving a Nucleophilic Attack to an Intermediary Formed from ^{1}[CP] State

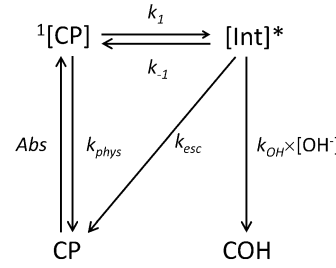

component (pre-exponential factor) is low, and the decay-time associated to DEACM−HPO_4^- is dominant. We believe to be a fair assumption that the photophysical and photochemical deactivation of DEACM−PO_4^{2-} are independent of the pH, as

evidenced by the constancy of the decay-times obtained in the pH region where this species dominates and its parallel behavior with DEACM−OH. From the data obtained at pH = 8.2 (fluorescence and photochemical quantum yields and decay-time), where only DEACM−PO_4^{2-} species is present in solution, the deactivation rate constants for the singlet excited state could be calculated and are presented in Table 1.

Photocleavage of DEACM−PO_4^{2-} is quite inefficient when compared to the other deactivation pathways. One might associate the increase in negative charge of the leaving group with an increase in the activation energy for the heterolytic cleavage, probably due to the electrostatic repulsion toward the incoming electron. This is reflected in a very low photocleavage quantum yield. Unexpectedly, DEACM−HPO_4^- decay-times show pH dependence, becoming progressively shorter with the increase of pH. Bendig and co-workers[6,13,14,22] proposed that an ion-pair is formed in the S1 state, followed by an escape, leading to ion-pair separation. Then, reaction with water molecules would lead to the alcohol photoproduct and free leaving group. No pH effect was considered.

For DEACM−HPO_4^-, if the overall decay rate constant (or the reciprocal of the short decay-time) is plotted as function of the hydroxyl anion concentration, a nonlinear dependence is found (Figure 7), which shows clearly that the hydroxyl (or proton) concentration has an effect in the excited state deactivating processes.

The nonlinear correlation between overall deactivating decay and hydroxyl concentration indicates that OH^- anion does not interact directly with S1 state of DEACM−HPO_4^-, referred hereafter as ^{1}[CP] for simplicity, through a S_N2 mechanism, involving direct nucleophilic attack by OH^-.

Three possible mechanisms were considered to explain the sigmoidal dependence of the excited state lifetime with the hydroxyl concentration: (i) equilibrium between ^{1}[CP] and a protonated excited state; (ii) quenching by the buffer; and (iii) hydroxyl attack to an intermediary species.

In a pH-dependent equilibrium affecting ^{1}[CP] (see Supporting Information, SI 2), protonation of the amine is expected to block the charge transfer and could account for the observed decrease of the overall rate with increasing proton concentration (if the protonated form has a shorter decay time). However, taking simple thermodynamic considerations based on the Förster cycle[24] and on spectroscopic data (the protonated form absorbs at higher energies—see Figure 2), excited state protonation (pK_a^*) is expected to occur only at pH values lower than 3.2 (ground state pK_a), seeming reasonable to exclude this mechanism on the pH range in question (pH 5 to 7).

A model in which the basic form of the buffer quenches the ^{1}[CP] state (see Supporting Information, SI 3) could also explain the sigmoidal dependence of the observed rate constant (since the buffer basic form concentration increases with increasing pH in a sigmoidal fashion). To test this hypothesis, we measured fluorescence decays at pH 5.62, 6.28, and 6.92 in phosphate buffer. The obtained decays are identical within the experimental error to those obtained in Tris-acetate buffer. The reciprocal of the short decay times (pH dependent rate constants) are plotted in Figure 7 (open circles), together with the data obtained in Tris-acetate. The existence of similar quenching in phosphate buffer excludes quenching by electron transfer. On the basis of this, it seems plausible to exclude buffer quenching as the source of the observed dependence.

It can also be considered the formation of a non emissive intermediary state, [Int]*, which reacts with hydroxyl anion (Scheme 1). This intermediary state can be a charge transfer state (CT), a close contact ion pair state (IP) or other chemical intermediary. [Int]* may react with the hydroxyl ion to produce the alcohol photoproduct with a bimolecular rate constant k_{OH}, or can alternatively be depopulated by pathways independent of [OH^-], included in the rate constant k_{esc}, according to Scheme 1.

The observed rate constant in this case is given by the following:

$$k_{obs} = \frac{k_1 \times k_{esc}}{k_{-1} + k_{esc} + k_{OH} \times [OH^-]} + \frac{(k_{-1} + k_{esc}) \times k_{phys}}{k_{-1} + k_{esc} + k_{OH} \times [OH^-]} + \frac{(k_1 + k_{phys}) \times k_{OH} \times [OH^-]}{k_{-1} + k_{esc} + k_{OH} \times [OH^-]} \quad (5)$$

At high [OH^-], $k_{obs} = k_{phys} + k_1$, which corresponds to the sum of the decay rates for ^{1}[CP] deactivation. At low [OH^-], $k_{obs} = (k_1 \times k_{esc})/(k_{-1} + k_{esc}) + k_{phys}$.

Several pairs of values of k_1 and k_{phys} can fit the data in Figure 7. However, no changes in the extinction coefficients of both DEACM−P species were observed within the studied pH range, and thus the radiative rate constant is expected to be identical for DEACM−HPO_4^- and DEACM−PO_4^{2-}. Also, the observed changes in fluorescence when going from DEACM−HPO_4^- to DEACM−PO_4^{2-} show a perfect correlation with the changes observed in the photochemistry. It is reasonable to assume that the nonradiative rate will not vary significantly within the studied pH range. Therefore, we believe to be a good approximation that the photophysical deactivation rate constant, k_{phys}, given by the sum of k_f and k_{nr}, will show a value close to the decay rate constant for DEACM−PO_4^{2-} at higher pH values (where the photochemistry is negligible). A value of 1.5×10^9 s^{-1} can be assumed for k_{phys}. A similar approximation was used by Schmidt et al.,[13] who additionally used the argument of effective electronic decoupling between the coumarinic chromophore and the O-bound substituent (e.g., phosphate) to assume that the nonradiative rate constants of the ester and the alcohol product were identical.

The sigmoidal shape of Figure 7 is only obtained if the sum $(k_{-1} + k_{esc})$ is of the same order of magnitude than that of k_{OH}[OH^-]. On one hand, $(k_{-1} + k_{esc}) \gg k_{OH}$[$OH^-$] leads to a linear dependence and, on the other hand, $(k_{-1} + k_{esc}) \ll k_{OH}$[$OH^-$] leads to an observed rate constant independent of [OH^-]. Nevertheless, several pairs of values for k_{OH}[OH^-] and $(k_{-1} + k_{esc})$ can also fit the data. If we assume the highest possible value for the bimolecular rate constant k_{OH}, i.e., its diffusional limit ($k_{OH} = 7 \times 10^9$ $M^{-1}s^{-1}$), calculated as the rate constant for a diffusion-controlled bimolecular reaction in water, using Fick's first law and the Stokes−Einstein equation,[25−27] the upper limit for the sum $(k_{-1} + k_{esc})$ that can be obtained with the presented mechanism is in the order of 10^3 s^{-1}. It should be noted that an unusual low pseudounimolecular rate constant (k_{OH}[OH^-]) is obtained since the hydroxyl concentrations are below 10^{-7} M.

As a consequence, and according to the proposed model (Scheme 1), if the intermediary state is a close contact ion pair and only electrostatic considerations are taken into account, the ion pair dissociation (which is included in the term $(k_{-1} + k_{esc})$) is predicted to occur with a rate constant $k_{diss} = 6.6 \times 10^8$ s^{-1} (calculated through the Eigen equation[28] — see Supporting Information, SI 4), and unless some strong (non electrostatic) interaction is present, which could prevent the ion pair dissociation (increasing its lifetime to the millisecond time scale), the ion pair intermediary may not seem plausible.

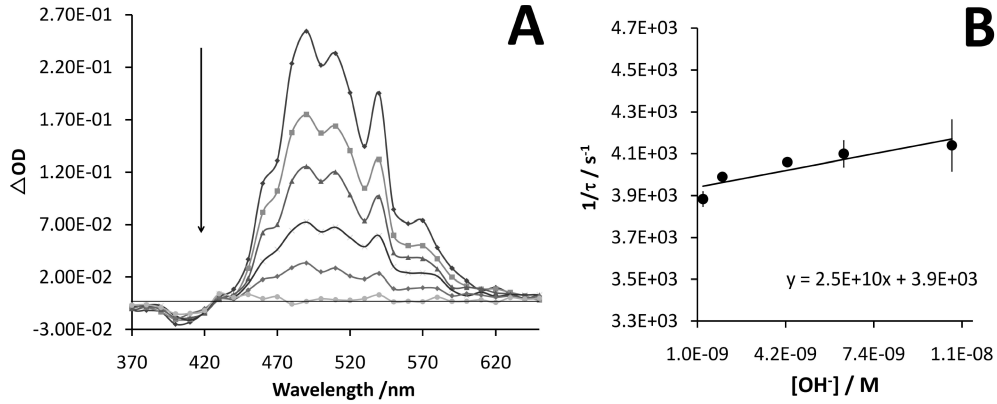

Figure 8. Flash Photolysis transient spectroscopy of DEACM−P. (A) Transient spectra of DEACM−P in 10 mM Tris-acetate buffer, pH 5.1, after 116, 196, 276, 396, 596, and 996 μs, respectively. Excitation was performed at 355 nm. (B) Observed rate constant given as the reciprocal of the decay time at 500 nm of DEACM−P as function of the hydroxyl concentration. Transient decays were obtained in 10 mM Tris-acetate buffer at the respective pH values, and excitation at 355 nm. The mean values of quintuplicate independent measurements are presented and error bars indicate the standard deviation from mean value.

Flash photolysis spectroscopy was performed in 10 mM Tris-acetate buffer, in the pH range between 5 and 6, where DEACM−HPO_4^- is the major species. A transient absorption with positive ΔOD is observed around 500 nm and a bleaching is observed at 390 nm that corresponds to the ground state absorption of DEACM−P (Figure 8A). The transient at 500 nm decays with a single exponential law with a pH dependent decay time spanning from 238 to 255 μs, while the bleaching at 390 nm recovers with a biexponential law (see Supporting Information, SI 5). The longer recovery time at 390 nm matches the decay time obtained at 500 nm, while the shorter recovery time is around 30 μs. Plotting the reciprocal of the decay times at 500 nm as a function of the hydroxyl concentration yields a linear correlation (Figure 8B; see Supporting Information, SI 6 for decays), compatible with a reaction between OH^- and the transient responsible by the 500 nm absorption. The intercept of the linear plot yields a value of 3.9×10^3 s^{-1}, and the slope indicates the presence of a diffusion limited rate constant with a value of 2.5×10^{10} $M^{-1}s^{-1}$. This constant is considerably higher than the value calculated by Fick's first law and Stokes−Einstein equation for the reaction of two neutral species and more in accordance with the prediction of the Debye−Smoluchowsky's equation[28] for the diffusion of oppositely charged species ($\sim 4 \times 10^{10}$ $M^{-1}s^{-1}$, see Supporting Information, SI 7). The value 2.5×10^{10} $M^{-1}s^{-1}$ was used as a fixed parameter for the fitting shown in Figure 7, which allowed to retrieve a value for ($k_{-1} + k_{esc}$) consistent with the intercept obtained in Figure 8B.

An additional observation is that the high diffusional constant determined indicates that the reaction is limited by the diffusion of two species of opposite charge, i.e., with hydroxyl anion attack to a cationic species (with the necessary cautions due to the very low hydroxyl concentration used and consequent experimental error). The nature of the cationic species is not known (radical cation, triplet or CT state, etc.) and further studies are needed to clarify this issue.

Conclusions

The pH produces significant variations in the photochemical quantum yield of (7-diethylaminocoumarin-4-yl)methyl phosphate (DEACM−P). The observed changes are complementary to those obtained from the fluorescence quantum yield, i.e., Φ_{chem} decreases with disappearance of the DEACM−HPO_4^- species to yield DEACM−PO_4^{2-}, while the fluorescence quantum yield increases. For DEACM−P, we show that a 14-fold overall decrease in the photochemistry quantum yield was due to deprotonation of the phosphate group. Furthermore, time-resolved fluorescence and flash photolysis experiments show that: (i) hydroxyl ion concentration affects S1 decay indirectly, possibly through an intermediary species formed in the first photochemical step; (ii) a long decay time transient was identified whose decay rate depends linearly on the hydroxyl ion concentration, consistent with the intermediary species; (iii) the intermediary is quenched by hydroxyl anion with a diffusional-limited rate constant; and (iv) the intermediary seems to present a cationic nature.

Our results show that special care must be taken with the operating pH range when ionizable coumarin-caged groups are concerned. Photochemical studies of 4-methylcoumarin ester derivatives have thus far systematically neglected this issue. Most living organisms and systems operate in tightly controlled pH conditions, usually in the range of pH 7.0−8.0. For example, in humans, pH varies according to the body or cell compartment within pH values of 7.35 and 8.20.[29] Enzymes react very sensitively to pH changes, with maximum activity (pH optimum) that coincides with the physiological pH value (about pH 7.4), and decreases significantly with slight pH variations (acid or alkaline). For in vitro enzymatic reactions, it is crucial to maintain the pH at constant values (pH 7−8) via appropriate buffer solutions.[30] Within this pH range, the concentration of the DEACM−HPO_4^- species, which presents higher photocleavage quantum yield, is almost negligible. The predominant species is DEACM−PO_4^{2-}, with a very low quantum yield, which accounted for the overall observed decrease of photocleavage with pH. The study of the absolute photochemistry magnitude of a given compound at a precise pH value is useless for in vivo applications, since the microenvironments inside cells are difficult to predict and might lead to dramatic changes in photochemical properties. We believe that the DEACM−P case study presented here can be of use for cage design toward application of 4-methylcoumarin ester derivatives in vivo or in vitro, and crucial for understanding the changes in photochemical quantum yields observed in vivo.

Acknowledgment. The authors would like to thank Dr. João Pina and Professor Sérgio S. Melo for the fluorescence lifetime measurements and Dr. Laura Raurell for the help in DEACM-P synthesis. The authors would like to thank Dr. César Laia for his help with the flash-flow setup and fruitful discussions. The

authors would like to acknowledge Fundação para a Ciência e Tecnologia for A. Vidal Pinheiro scholarship SFRH/BD/24276/2005.

Supporting Information Available: Picosecond fluorescence decays, kinetic models accounting for excited state protonation and quenching by the buffer, estimates of ion pair dissociation and ion pair diffusion encounter rate constants, flash photolysis decays. This information is available free of charge via the Internet at http://pubs.acs.org.

References and Notes

(1) Kapland, J. H.; Forbush, B.; Hoffman, J. F. *Biochemistry* **1978**, *17*, 1929–1935.

(2) Adams, S. R.; Tsien, R. Y. *Annu. Rev. Physiol.* **1993**, *55*, 755–784.

(3) Furuta, T.; Noguchi, K. *TrAC, Trends Anal. Chem.* **2004**, *23*, 511–519.

(4) Mayer, G.; Heckel, A. *Angew. Chem., Int. Ed.* **2006**, *45*, 4900–4921.

(5) Pelliccioli, A. P.; Wirz, J. *Photochem. Photobiol. Sci.* **2002**, *1*, 441–458.

(6) Schade, B.; Hagen, V.; Schmidt, R.; Herbrich, R.; Krause, E.; Eckardt, T.; Bendig, J. *J. Org. Chem.* **1999**, *64*, 9109–9117.

(7) Taniguchi, A.; Skwarczynski, M.; Sohma, Y.; Okada, T.; Ikeda, K.; Prakash, H.; Mukai, H.; Hayashi, Y.; Kimura, T.; Hirota, S.; Matsuzaki, K.; Kiso, Y. *ChemBioChem* **2008**, *9*, 3055–3065.

(8) Geiβler, D.; Antonenko, Y. N.; Schmidt, R.; Keller, S.; Krylova, O. O.; Wiesner, B.; Bendig, J.; Pohl, P.; Hagen, V. *Angew. Chem., Int. Ed.* **2005**, *44*, 1195–1198.

(9) Furuta, T.; Wang, S. S.; Dantzker, J. L.; Dore, T. M.; Bybee, W. J.; Callaway, E. M.; Denk, W.; Tsien, R. Y. *Proc. Natl. Acad. Sci. U.S.A.* **1999**, *96*, 1193–1200.

(10) Ando, H.; Furuta, T.; Tsien, R. Y.; Okamoto, H. *Nat. Genet.* **2001**, *28*, 317–325.

(11) Hagen, V.; Bendig, J.; Frings, S.; Eckardt, T.; Helm, S.; Reuter, D.; Kaupp, U. B. *Angew. Chem., Int. Ed.* **2001**, *40*, 1046–1048.

(12) Hagen, V.; Frings, S.; Wiesner, B.; Helm, S.; Kaupp, U. B.; Bendig, J. *ChemBioChem* **2003**, *4*, 434–442.

(13) Schmidt, R.; Geiβler, D.; Hagen, V.; Bendig, J. *J. Phys. Chem. A* **2005**, *109*, 5000–5004.

(14) Schmidt, R.; Geiβler, D.; Hagen, V.; Bendig, J. *J. Phys. Chem. A* **2007**, *111*, 5768–5774.

(15) Schonleber, R. O.; Bendig, J.; Hagen, V.; Giese, B. *Bioorg. Med. Chem.* **2002**, *10*, 97–101.

(16) Du, H.; Fuh, R. A.; Li, J.; Corkan, A.; Lindsey, J. S. *Photochem. Photobiol.* **1998**, *68*, 141–142.

(17) Montalti, M.; Credi, A.; Prodi, L.; Gandolfi, M. T. *Handbook of Photochemistry*, 3rd ed.; CRC Press, Taylor and Francis Group: Boca Raton, FL, USA, 2006.

(18) Pina, J.; Seixas de Melo, J.; Burrows, H. D.; Maçanita, A. L.; Galbrecht, F.; Bunnagel, T.; Scherf, U. *Macromolecules* **2009**, *42*, 1710–1719.

(19) Striker, G. *Deconvolution and Reconvolution of Analytical Signals*; University Press: Nancy, 1982.

(20) Striker, G.; Subramaniam, V.; Seidel, C. A. M.; Volkmer, A. *J. Phys. Chem. B* **1999**, *103*, 8612.

(21) Vidal Pinheiro, A.; Baptista, P.; Lima, J. C. *Nucleic Acids Res.* **2008**, *36*, 90.

(22) Eckardt, T.; Hagen, V.; Schade, B.; Schmidt, R.; Schweitzer, C.; Bendig, J. *J. Org. Chem.* **2002**, *67*, 703–710.

(23) Kumler, W. D.; Eiler, J. J. *J. Am. Chem. Soc.* **1943**, *65*, 2355–2361.

(24) Rohatgi-Mukherjee, K. K. *Fundamentals of Photochemistry, Revised Ed.*; Wiley Eastern Limited: New Deli, India, 1986.

(25) Atkins, P. W. *Physical Chemistry*, 4th ed.; Oxford University Press: Oxford, United Kingdom, 1990, p 848, equation 7.

(26) Lide, R. D. *CRC Handbook of Chemistry and Physics*, 72nd ed.; CRC Press, Inc.: Boca Raton, USA, 1991.

(27) Edward, J. T. *J. Chem. Educ.* **1970**, *47*, 261–270.

(28) Billing, R.; Rehorek, D.; Hennig, H. Photoinduced Electron Transfer in Ion Pairs. In *Photoinduced Electron Transfer II, Topics of Current Chemistry*; Mattay, J., Ed.; Springer-Verlag: Berlin Heidelberg, Germany, 1990, Vol *158*.

(29) Boron, W. F.; Boulpaep, E. L. *Medical Physiology: A Cellular and Molecular Approach*; Elsevier/W. B. Saunders Company: St. Louis, MO, USA, 2004.

(30) Bisswanger, H. *Enzyme Kinetics—Principles and Methods*; Wiley-VCH: Verlag GmbH, Germany, 2002.

JP103045U